Mechanical Properties of Cu-MWCNT Composites Developed by Powder Metallurgy Route

Lailesh Kumar, Syed Nasimul Alam, Santosh Kumar Sahoo, M. B. K. Teja*

Department of Metallurgical and Materials Engineering, National Institute of Technology Rourkela, Rourkela, Odisha, Pin-769008, India

Abstract

Cu-based composites reinforced by MWCNTs were developed by PM route and their microstructure, mechanical properties, sliding wear behaviour and crystallographic texture was investigated. The MWCNTs were synthesized by LPCVD technique and was functionalized using acid modification route. Cu-1, 2 and 3 wt. % MWCNT composites were developed by blending the Cu and MWCNTs powders which were later consolidated under a uniaxial load of 565 MPa and sintered at 850°C for 2 h in Ar atmosphere. A significant improvement in relative density, microhardness and wear resistance of the composites was observed up to the addition of 2 wt. % of MWCNTs.

Keywords: Cu-based metal matrix composites; MWCNT; Powder metallurgy; Wear; Residual stress; Crystallographic texture

Introduction

Copper (Cu) has a wide range of applications due to its excellent thermal and electrical properties. Cu-based metal matrix composites (MMCs) have application in areas where good wear resistance without the loss of electrical and thermal conductivity of the matrix is essential. Cu-based MMCs developed by powder metallurgy (PM) route are widely used in the manufacturing of tribological engineering parts such as bearings and bushes. Cu has a wide range of excellent properties like high electrical conductivity (5.98×10^6 S/m), high thermal conductivity (401 $W\cdot m^{-1}\cdot K^{-1}$) and excellent corrosion resistance. The melting point of Cu is 1083.4°C, and its density is 8.96 gm/cc. The Young's modulus of Cu is 130 GPa, its yield strength is 117 MPa while its tensile strength is 210 MPa. However, the main drawback of Cu is its relatively low strength and in order to increase its high-temperature properties, different reinforcements are being used [1-3]. Carbon nanotubes (CNTs), since their discovery, have been used as nanofiller for the development of a variety of composites. Al and Mg-based MMCs reinforced with CNTs have been developed for use as lightweight structural materials [4, 5]. CNTs provide a new avenue for the reinforcement of Cu-based materials. They can not only help in retaining the properties of the Cu matrix but also enhance the mechanical, electrical and thermal properties of Cu. However, work on Cu-based MMCs using CNTs as reinforcement is still relatively new and very few reports in this area are available in the literature [6, 7]. CNTs have a tubular structure made of carbon atoms, having a diameter of nanometer order and length of several microns. Its modulus is in the range of 0.3-1 TPa, and its tensile strength is in the range of 10-60 GPa. Its electrical conductivity is 10^6-10^7 **S/m,** and its thermal conductivity is 3000 W/m.K. It has a density of around *2.6 gm/cc, and possess a high* specific surface area in the range of 200-400 m^2/gm. CNTs have high aspect ratio, chemical inertness, and structural stability [8-10]. However, it has still not been possible to translate the unique mechanical properties of CNTs into bulk composites by using them as reinforcements. The realization of nanoscale properties in bulk materials is still a challenging problem. It has been reported earlier that Cu-based MMCs reinforced with CNTs have superior mechanical properties and are more thermally stable compared to pure Cu. Cu-based MMCs having carbon nanotubes as nanofiller could be used as structural as well as functional materials because of their extraordinary strength and excellent electrical and thermal conductivity. Cu-MWCNT composites would make attractive novel materials with potential application in various areas like aerospace, automotive, spaceflight and sports industries where light weight combined with high stiffness and strength is desired. Powder metallurgy (PM) is the most preferred technique adopted for the development of MMCs reinforced with nanofillers like CNTs as this technique enables efficient dispersion of the CNTs in the metal matrix. The PM technique also provides enormous flexibility during the different stages of composite processing [11, 12]. In the present study Cu-1, 2, 3 wt. % MWCNT composites were developed by the PM technique and subsequently, the effect of MWCNT on the mechanical properties, wear behaviour, residual stress development and crystallographic

* Corresponding author. Tel.: +91-661-2462563;
E-mail address: krupateja0797@gmail.com

texture of the composites were investigated. Cu-MWCNT composites would give significantly improved mechanical and tribological properties. Here, an attempt has also been made to correlate the crystallographic texture and the residual stress development with the mechanical properties and the wear behavior of the composites.

2. Experimental Method

Elemental Cu powder having purity > 99% and average particle size of ~25 µm was procured from Loba Chemie. The fabrication of the various Cu-MWCNT composites has been realized by PM route. The Cu and MWCNT powder were initially blended in the proper weight fraction and the blended powder was later cold compacted under a uniaxial load of 565 MPa. This is followed by sintering of the compacts in Ar atmosphere in a tubular furnace at 850°C for a period of 2 h. Cu - 1, 2, 3 wt. % MWCNT composites were developed. The sintered Cu-MWCNT composites were characterized using a Panalytical PW 3040 X'Pert MPD X-ray diffractometer using Cu K_α radiation (λ = 1.541 Å). The mulitwalled carbon nanotubes (MWCNTs) used here as a nanofiller for the development of the Cu-MWCNT composites have been synthesized by a low pressure chemical vapour deposition (LPCVD) technique.

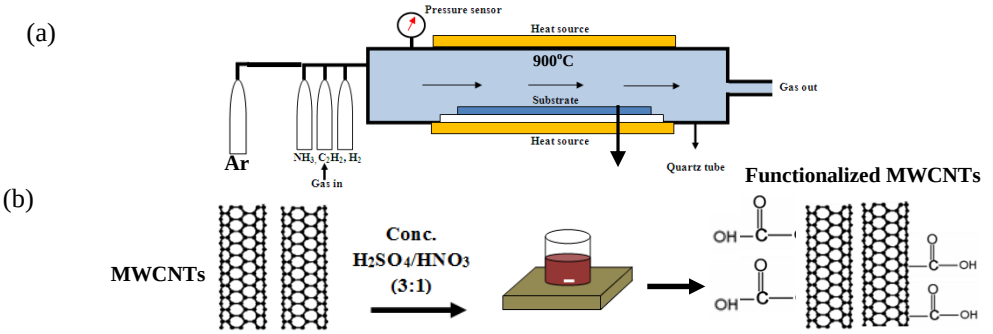

Fig. 1 (a) LPCVD furnace setup (b) Various steps for the functionalization of MWCNTs.

For the synthesis of the MWCNTs by the LPCVD process, a Fe-thin film catalyst having a thickness of ~15 nm was deposited on a Si substrate using RF sputtering (MODEL: 12" MSPT) at a power of 50 W and argon (Ar) pressure of $1x10^{-3}$ Torr. The sputtered film was then cleaned ultrasonically in acetone and dried at room temperature. The Si substrate coated with the Fe-thin film was later heated under a flow of H_2 gas in a high-temperature tubular furnace. A mixture of H_2:C_2H_2:NH_3 with flow rates of 50:20:50 sccm respectively was then passed through the quartz tube. The reaction temperature was maintained at 900°C and the growth time was 20 minutes. To prevent oxidation and removal of gaseous byproducts Ar gas was fed at a controlled rate of 600 sccm during the entire heating up, growth and cooling down periods. A detailed schematic diagram of the LPCVD furnace setup used for the synthesis of the MWCNTs is shown in Fig.1 (a). In order to avoid the agglomeration of the MWCNTs in the composites, the MWCNTs have been functionalized using an acid modification route. Avoiding agglomeration of the nanofillers during the development of the composites is a major challenge. The MWCNTs were stirred using a magnetic stirrer for 8 h in an acidic solution containing H_2SO_4 and HNO_3 in 3:1 ratio having 50 % acid concentration. The MWCNTs were then filtered and repeatedly washed using distilled water until the pH value of 7 was attained. The MWCNTs were then dried in a vacuum oven at 80°C for 5 h. The Van der Waal's forces between the MWCNTs are overcome by the presence of carboxyl (COOH) and hydroxyl (OH) groups which have been introduced during functionalization and prevent their agglomeration. The schematic diagram in Fig.1 (b) shows the various steps adopted for the functionalization of the MWCNTs. Scanning electron microscopy (SEM) of the MWCNTs and the various sintered samples were carried out using a JEOL JSM-6480LV SEM. The MWCNTs and the various sintered composite samples were also analyzed by employing a JEOL JEM-2100 high-resolution transmission electron microscope (HRTEM). The dry sliding wear test of the various sintered samples was performed using a Ducom ball-on-plate tribometer. The wear test of the various sintered composites was conducted at a speed of 20 rpm under a load of 15 N for 10 minutes. The hardness of the various samples was determined using a Leeco Vickers microhardness tester. The tensile tests of the various sintered composites was performed using an Instron 1195 universal testing machine (UTM). The residual stress and texture analysis of the sintered samples were done using a Bruker D8 Advance X-ray diffraction system. The (111), (200) and (220) poles were determined and the orientation distribution function (ODF)

was analyzed using the Labotex 3.0 software. The standard $Sin^2\Psi$ method has been used for determining the residual stress in the samples.

3. Results and Discussion

Figs.2 (a, b) are the SEM images of the Cu powder that has been used for developing the various Cu-MWCNT composites. The Cu powder shows a dendritic structure and the EDX analysis of the Cu powder along with the SEM image in Fig. 2(a) suggests that it is 100 % Cu. From the SEM images of the MWCNTs in Figs. 2(c, d) it is evident that the MWCNTs are 20-35 nm in diameter and have lengths of upto 1-2 µm. Due to the high aspect ratio of the MWCNTs and their tendency to agglomerate, deagglomeration of the MWCNTs is a major challenge. The MWCNTs have been acid functionalized in order to avoid their agglomeration and achieve uniform dispersion of the MWCNTs in the metal matrix.

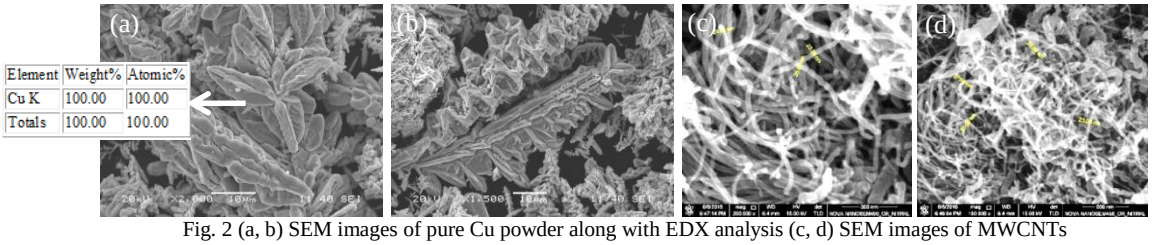

Fig. 2 (a, b) SEM images of pure Cu powder along with EDX analysis (c, d) SEM images of MWCNTs

HRTEM investigation was performed to determine the morphology of the MWCNTs. Figs.3 (a-d) are the HRTEM images and Fig. 3(e) is the SAD pattern of the MWCNT synthesized by LPCVD process. The multiwalled structure of the MWCNTs is clearly evident from the HRTEM images. From Figs.3 (c, d) it is revealed that the hollow central portion of the MWCNT is about 10 nm in diameter and the outside diameter is ~25 nm. The wall thickness of the MWCNTs was found to be ~10 nm. Fig.3 (d) shows that the graphite layer lattice fringes parallel to the nanotube axis. A significant number of Fe particles that had been used as a catalyst during the synthesis of the MWCNTs by the LPCVD process could not be found in the HRTEM images suggesting the high purity of MWCNTs. The SAD image in Fig.3 (e) shows concentric ring pattern which indicates the nanometric dimension of the MWCNTs.

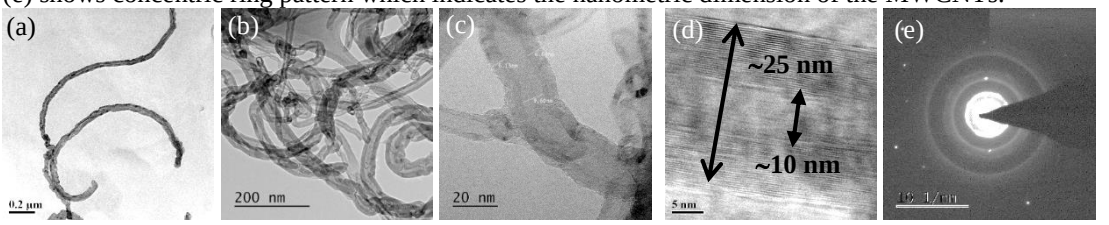

Fig. 3 (a-d) HRTEM images and (e) SAD pattern of MWCNTs

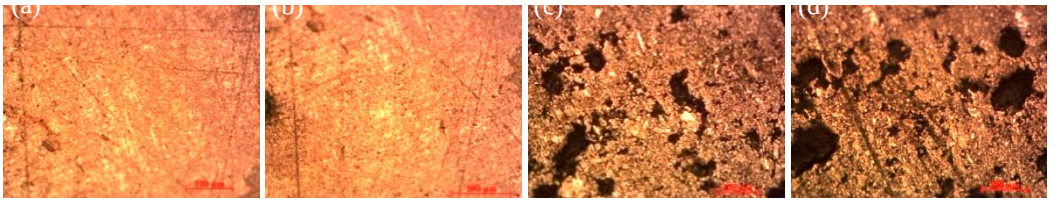

Fig. 4 Optical images of (a, b) Cu-1 wt. % MWCNT composite and (c, d) Cu-3 wt. % MWCNT composite

The optical micrographs of Cu-1 and 3 wt. % MWCNT composite in Figs. 4(a, b) and Figs. 5(c, d) respectively show that there is a homogeneous dispersion of MWCNTs throughout the Cu matrix. The MWCNTs are evenly distributed throughout the Cu matrix, and there is no evidence of agglomeration in these samples. As the loading level of the nanofiller is increased their distribution in the Cu matrix reduces and shows a higher tendency to agglomerate. The optical micrographs of Cu-3 wt. % MWCNT composite in Figs.4 (c, d) show dark coloured lumps having a size of around ~ 80 µm.

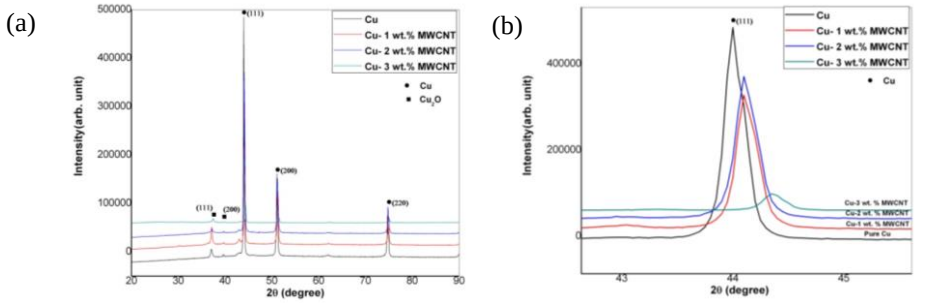

Fig. 5 (a) XRD of sintered pure Cu and various Cu-MWCNT composites (b) XRD in the range of 2θ = 42-46º

Fig.5(a) shows the XRD patterns of sintered pure Cu and the various Cu-MWCNT composites containing different wt. % of MWCNTs. Peaks corresponding to the (111), (200) and (220) planes of FCC Cu could be seen in the XRD plot. The most intense (002) peak of MWCNTs at the 2θ value of 26.4º is not visible in the XRD plot of any of the composites due to the low concentration of the MWCNTs. It should be noted that the intensity of the various diffraction peaks of Cu in the Cu-MWCNT composites is found to be lower than that of the pure Cu (Fig. 5(b)). The attenuation of the intensity of the various diffraction peaks of Cu with the addition of MWCNTs can be attributed to the decrease in the grain size of Cu in the various Cu-MWCNT composites. The MWCNTs present at the grain boundaries restrict the growth of the Cu grains during sintering resulting in finer grains of Cu. Few peaks corresponding to copper oxide (Cu_2O) could also be seen in the XRD plots of all the composites due to the oxidation of Cu by the residual oxygen present during sintering [15, 16]. No new phase formed due to the reaction between Cu and the MWCNTs could be seen in the XRD plots [17].

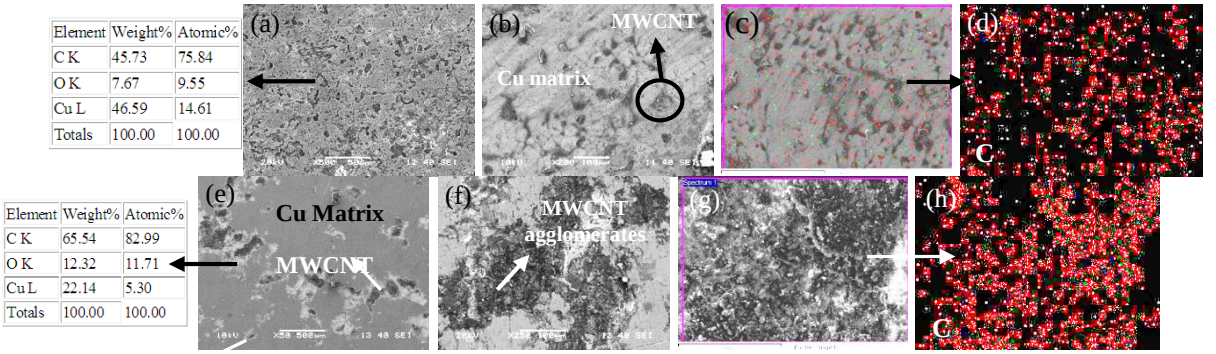

Fig. 6 (a-c) SEM images with EDX analysis and (d) elemental map of C in Cu-1 wt. % MWCNT composite. (e-g) SEM images with EDX analysis and (h) elemental map of C in Cu-3 wt. % MWCNT composite.

The SEM images in Figs. 6(a-c) of Cu-1 wt. % MWCNT composite also shows a uniform distribution of MWCNTs in the Cu matrix which was also seen in the optical micrographs in Figs. 4(a, b). The MWCNTs are evenly distributed throughout the Cu matrix, and there is no evidence of agglomeration in these samples. The dark regions in the Cu-1 wt. % MWCNT composite in Figs. 6(a-c) are the MWCNTs embedded in the Cu matrix. As can be seen from the SEM images in Figs.6 (a-c) an interconnecting network of MWCNTs is formed in the case lower loading level of the MWCNTs. The SEM image in Fig.6 (a) clearly indicates that the CNTs are mainly distributed at the grain boundaries. The carbon nanotubes present at the grain boundaries very effectively hinder the grain growth and thereby results in very fine Cu grains homogenously distributed in the matrix. The presence of the MWCNTs at the grain boundaries inhibit dislocation nucleation and motion, resulting in an increase in the strength of the composite [18]. The EDX analysis along with the SEM image in Fig.6 (a) confirms the presence of Cu, C and O in the Cu-1 wt. % MWCNT composite. The elemental map of C in Fig.6 (d) clearly indicates the homogeneous distribution of the MWCNTs in the Cu matrix. The SEM images of Cu-3 wt. % MWCNT composite in Figs.6 (e-g) show large agglomerates of MWCNTs in the Cu matrix suggesting that addition of higher wt. % of MWCNT could lead to agglomeration of MWCNTs in the Cu matrix. The optical micrographs of Cu-3 wt. % MWCNT composite in Fig.4(c, d) also show large agglomerates of MWCNTs in the Cu matrix. The elemental map of C in Fig.6 (h) also shows dense regions of

MWCNTs in the Cu matrix.

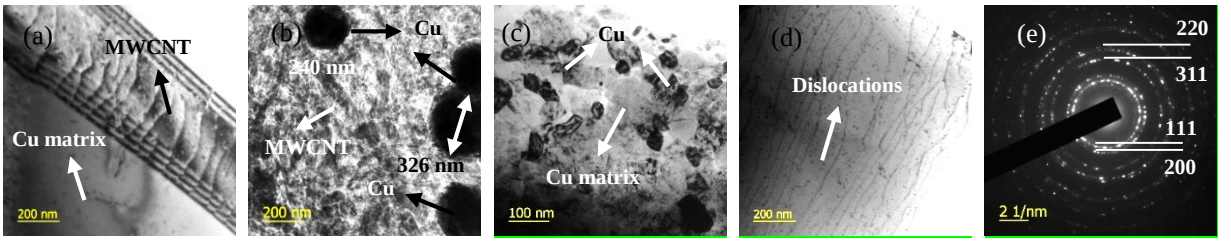

Fig. 7 (a-d) HRTEM images and (e) SAD pattern of the Cu-3 wt. % MWCNT composite

The performance of a composite depends on the dispersion of the nanofiller in the matrix. The dispersion of the MWCNTs in the Cu matrix was investigated using HRTEM. HRTEM micrographs of Cu-3 wt. % MWCNT composite were collected to gain a better understanding of the MWCNT dispersion in the Cu matrix. The HRTEM images of the Cu-3 wt. % MWCNT composites in Figs. 7(a-c) reveal that the MWCNTs are embedded in the Cu matrix and maintained their structure even after the sintering of the composite. The structure of the MWCNTs has been preserved during the development of the composite, although a few agglomerations and breakdown of MWCNTs could be observed. No gaps could be found at the interface of the MWCNTs and the Cu matrix indicating a strong interaction between the Cu particles and the carbon nanotubes. In the HRTEM images well dispersed spherical Cu particles could be seen anchored to the external walls of the carbon nanotubes or trapped within the multiwalled structures of individual nanotubes. Carbon nanotubes were found at the Cu grain boundaries. A large number of Cu particles, irregularly distributed on the surfaces of the MWCNTs having sizes in the range of 200-300 nm could be seen in Figs. 7(b, c). A large number of dislocations piled up along a plane could be observed in Fig. 7(d) in the interior of the Cu grains. The Cu grains are highly strained and contain a high density of dislocations. The pinning effect of the MWCNTs leads to a large number of dislocations in the Cu grains. The pinning effect also resulted in the decrease of the Cu grain size. The decrease in grain size of Cu with the addition of MWCNTs was also confirmed by the XRD analysis in Fig.5 (b). The rings in the SAD pattern of Cu-3 wt. % MWCNT composite in Fig.7 (e) could be indexed to the various planes of Cu. The bright rings with occasional bright spots in the SAD pattern signify the crystalline nature of the Cu matrix [19, 20].

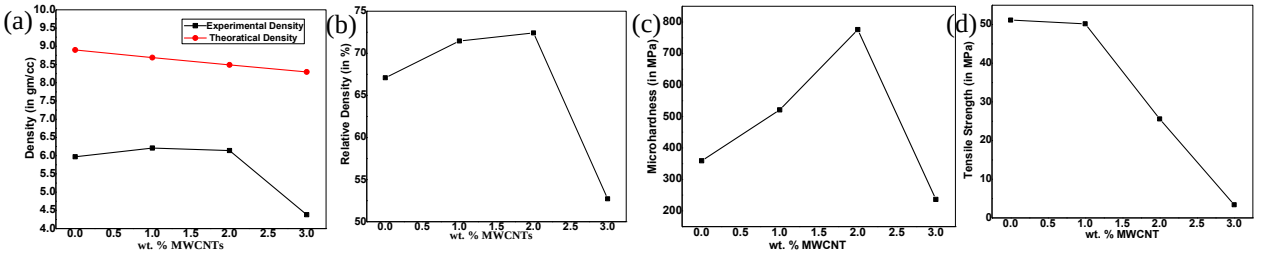

Fig. 8 Variation of (a) theoretical and experimental density (b) relative density (c) microhardness and (d) tensile strength of sintered Cu-MWCNT composites with MWCNT content

The theoretical density of the various Cu-MWCNT composites was calculated using the rule of mixtures. The density of MWCNT was considered as 2.6 gm/cc, and the density of Cu was considered as 8.9 gm/cc. Fig. 8(a) shows the variation of theoretical and experimental density with the increase in the content of MWCNT in the Cu-MWCNT composites. It is evident from the plot in Fig.8 (a) that both the theoretical and experimental density of the Cu-MWCNT composites reduces with the addition of MWCNTs in the Cu matrix. As the density of MWCNT is lower than the density of pure Cu. Therefore the addition of MWCNT results in a lower density of the Cu-MWCNT composites as compared to that of pure Cu. Fig.8 (b) shows the variation of relative density of Cu-MWCNT composites with the addition of MWCNT reinforcement. It can be observed that the relative density initially increases with the increase in the content of MWCNTs in the Cu matrix. The carbon nanotubes very effectively fill up the microvoids in the Cu matrix leading to enhanced sinterability and densification of the composites. However, it does not show any increase in densification after addition of more than 2 wt. % of MWCNTs in the Cu matrix and the

relative density of the composite reduces. It should be noted that there is a good bonding between the Cu matrix and the MWCNTs due to the acidic treatment of the MWCNTs during functionalization which produces active sites providing better wettability. The relative density of Cu-3 wt. % MWCNT composite was lower than that achieved in the case of pure Cu due to agglomerations of MWCNTs at the grain boundaries of the Cu matrix which leads to the formation of pores. These agglomerates are increased with the increase in the content of MWCNTs. The hardness of both sintered pure Cu and the various Cu-MWCNT composites was determined using a Vickers microhardness tester. The hardness values were measured on polished samples of the various composites. It can be seen from the plot in Fig.8(c) that the hardness of the Cu-MWCNT composite is higher than that of the sintered pure Cu when the MWCNT content in the composite is upto 2 wt. %. The hardness of Cu-MWCNT composites increases almost linearly with the increase in MWCNT content up to the addition of 2 wt. % MWCNT in the Cu matrix. When 2 wt. % of MWCNTs is added to the Cu matrix the hardness of Cu-MWCNT composite was found to be 775 MPa, which is about 2.15 times that of the sintered pure Cu sample. This can be attributed to the effect of the homogeneous distribution of the MWCNTs in the Cu matrix and the high interfacial strength that results due to the good bonding at the interface of the functionalized MWCNTs and the Cu matrix. The introduction of carboxyl and hydroxyl groups on the surface of the MWCNTs during functionalization provides binding sites for the Cu matrix to the MWCNTs. Carbon nanotubes can withstand much higher loads than the Cu matrix and hence there is a substantial increase in the hardness values [21, 22]. However, beyond 2 wt. % of MWCNT the hardness of the composite decreases due to the agglomeration of the MWCNTs in the Cu matrix. The agglomeration of MWCNTs in the Cu-3 wt. % MWCNT composite was also evident from the optical and SEM images of the composite in Figs.4(c, d) and Figs.6(e-g) respectively. The tensile tests of the various Cu-MWCNT composites were done to find out the effect of the addition of MWCNTs on the tensile properties of the composites. Fig.8 (d) shows the variation of the tensile strength of the various Cu-MWCNT composites. There is a gradual decrease in the tensile strength of the composites with the increase in MWCNT in the Cu matrix. As the concentration of the MWCNT increases, it leads to the formation of an interconnected network that acts as an interface. The decrease in tensile strength is due to the increase in the number of sites of interconnected MWCNTs with increasing MWCNT content. The formation of an interconnecting network of MWCNTs promoted easy fracture of the composites [23]. The decrease in tensile strength can also be attributed to the presence of voids which act as brittle weakness. The dispersion of MWCNTs in the Cu matrix plays an important role in enhancing the wear resistance of the Cu-MWCNT composites.

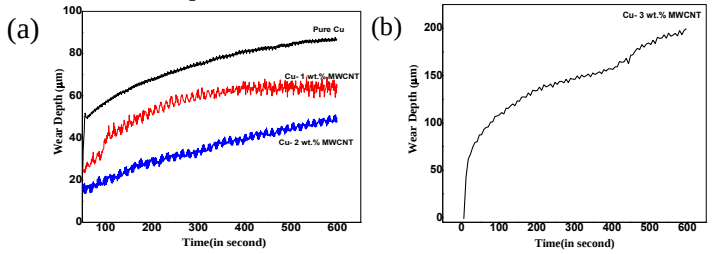

Fig. 9 Variation of wear depth for (a) pure Cu , Cu-1, 2 wt. % MWCNT and (b) Cu-3 wt. % MWCNT composite

The wear characteristics of the Cu-MWCNT composites shown in Fig.9 indicates that the wear resistance of the composite increases with the increase in the loading level of the MWCNTs. The MWCNTs act as a lubricating carbon film. The low coefficient of friction of the MWCNTs leads to higher wear resistance of the composites. However, higher loading level of MWCNTs leads to a reduction in direct contact between the Cu matrix and the indenter thereby resulting in lower wear resistance of the composites. Fig.9 shows the variation of wear depth with time for pure Cu and Cu-1, 2 and 3 wt. % MWCNT composites. The wear resistance of the Cu-MWCNT composite was found to improve upto the addition of 2 wt. % MWCNT. Better homogeneity of the MWCNT in the Cu matrix leads to a lower coefficient of friction of the Cu-MWCNT composites. The multilayer structure of the MWCNTs provides a lubricating effect to the Cu matrix due to which the friction between the diamond indenter and the composites is less during the wear test [24, 25]. However, we see a reduction in the wear resistance of the composite leading to an increase in the wear depth in the case of Cu-3 wt. % MWCNT composite due to the agglomeration of MWCNTs in the Cu matrix. As the Cu-matrix gradually flaked during the wear test, the MWCNTs in the matrix near the surface were exposed and became the working film on the worn surface. The worn contacting surfaces were thus changed from the original metal surfaces into metals with lubricating carbon nanotubes. This significantly reduced the adhesion between the composite and the counterpart. An oxide film is formed at the interface between the indenter of the wear tester and

sample due to the heat generated during the wear test which causes the temperature of the specimen to rise. During the wear test O_2 is reduced to O^- and O^{2-} and thereby oxidizes Cu to copper oxides like CuO or Cu_2O which forms an oxide film on the surface of the sample. However, it should be noted that as carbon is easier to oxidize as compared to Cu, the MWCNTs get oxidized readily to form CO and CO_2 and retards the formation of CuO and Cu_2O during the wear test [26, 27]. Thus the MWCNTs not only act as a lubricant but it also prevents the Cu matrix from oxidation during the wear process.

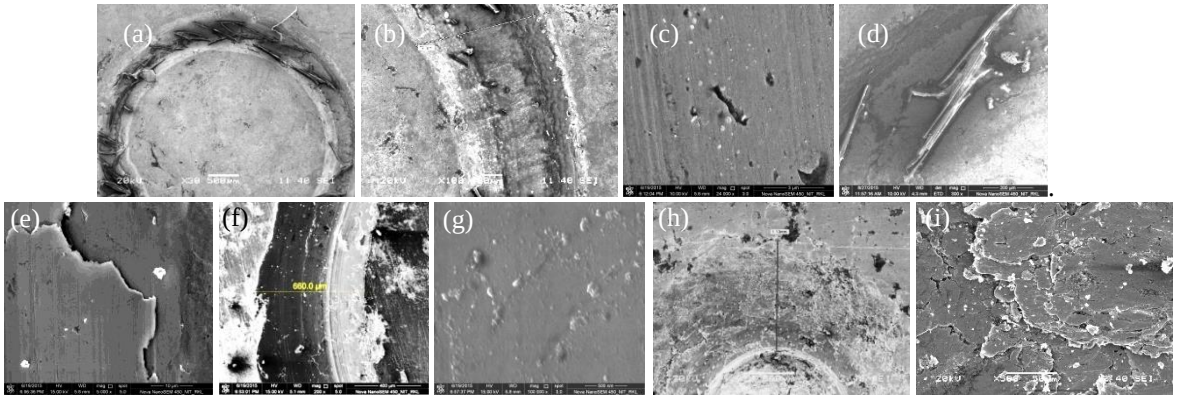

Fig. 10 SEM images of the wear track of (a-d) Cu-1 wt. % MWCNT (e, f) Cu-2 wt. % MWCNT (g, h) Cu-3 wt. % MWCNT composite

From the SEM images of the wear track of the various Cu-MWCNT composites in Fig. 10 the wear mechanism was found to involve a combination of abrasion, ploughing, delamination, microcracks and pullout of MWCNTs. The width of the wear track gradually reduces upto the addition of 2 wt. % MWCNT. However, an increase in the width of the wear track was found in the case of Cu-3 wt. % MWCNT composite. This is due to the agglomeration of MWCNTs in the Cu matrix. The SEM images in Figs.10 (h, i) show that there are some flake-like wear scars on the wear track of the Cu- 3 wt. % MWCNT composite, which are typical characteristics of abrasive wear [28, 29]. The XRD plot in Fig. 11(a) of the wear debris from the wear track of Cu-3 wt. % MWCNT composite shows peaks corresponding to the (002) diffraction plane of MWCNT. Apart from this peaks corresponding to the various planes of Cu could also be seen in the XRD plot of the wear debris which suggests that both MWCNT and Cu are present in the wear debris of the Cu- 3 wt. % MWCNT composite. The XRD result also shows peaks corresponding to Cu_2O in the wear debris of the composite. This suggests that oxidation wear is one of the main wear mechanisms. Both MWCNTs and Cu were found in the wear debris from the wear track of Cu - 3 wt. % MWCNT in Figs.11 (b, c). Flake-like flattened Cu particles could be seen in the SEM image of the wear debris in Fig. 11(b). MWCNTs are clearly visible in the SEM image in Fig. 11(c).

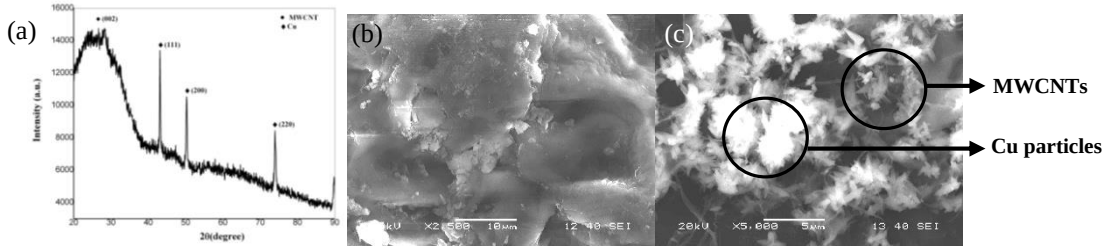

Fig. 11 (a) XRD and (b, c) SEM images of the wear debris from the wear track of Cu-3 wt. % MWCNT composite

The fracture surfaces of sintered pure Cu and the various Cu-MWCNT composites fractured by tensile test were analyzed in SEM. From the fractographs of both pure Cu in Fig. 12(a) as well as that of the various Cu-MWCNT composites in Figs.12 (b-d) it evident that the fracture is ductile in nature in all the composite samples. Dimples could be clearly seen in all the fractured samples. Fig.12 (a) is the SEM image of the fracture surface of the sintered pure Cu sample. Dimples could be seen on the fracture surface along with dark pores. These pores left behind during compaction and subsequent sintering are responsible for the initiation of fracture. Cavities are also seen in the SEM

image in Fig. 12 (b) where the MWCNTs have been pulled out from the metal matrix during the tensile test. The SEM images of the fracture surfaces also show MWCNTs trapped between the Cu grain boundaries. Pull-out of MWCNTs from the metal matrix could also be observed on the fracture surface. MWCNTs could be seen protruding from the fracture surface (Figs.12 (c, d)). The SEM images also show regions where nanotubes are agglomerated as well as embedded in the Cu matrix. The amount of embedded MWCNTs was found to increase with the increase in the content of MWCNTs in the composites. The MWCNTs due to their high aspect ratio contribute more to the bridging effect which obstructs the propagation of the crack. It is known that MWCNTs can be stretched before collapsing during crack propagation. The strengthening mechanism can be explained by the uncoiling and stretching of the carbon nanotubes. The uncoiling and stretching of the carbon nanotubes produce friction and dissipate energy at the crack tip and as a result, increases the toughness of the composites. During intergranular crack propagation, the entangled carbon nanotube bundles are first uncoiled. With further propagation of the crack, the uncoiled nanotubes stretch while their ends are anchored within the grains of the metal matrix. This results in crack bridging and obstructs the propagation of the crack. Finally, the nanotubes separate from the metal matrix interface [30, 31].

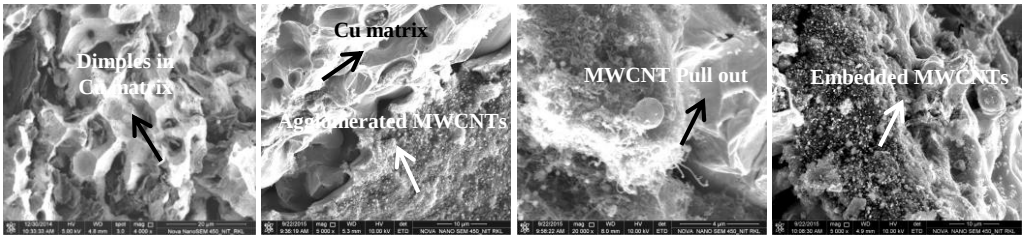

Fig. 12 SEM images of the fracture surface of sintered (a) pure Cu (b) Cu-1 wt. % MWCNT (c) Cu-2 wt. % MWCNT (d) Cu-3 wt. % MWCNT composites

Fig.13 shows the orientation distribution function (ODF) maps at constant ϕ_2=0° in pure Cu and the various Cu-MWCNT composites. The initial texture of the pure Cu sample before addition of the reinforcement is found to be very strong (Fig. 13(a)). A dominant <011> fiber texture is seen in the sintered pure Cu as well as the various Cu-MWCNT composites. However, the intensity of the fiber is weakened with the addition of the MWCNTs (Figs. 13(b, c)) [32]. The volume fraction of <011> fibre as a function of MWCNTs shown in Fig. 13(d) shows a decreasing trend in the volume fraction of <011> fibre. However, a rise in the volume fraction of <011> fibre was observed beyond 2 wt. % of MWCNTs in the matrix. A distinct <010> fibre was also seen in pure Cu sample before addition of the MWCNTs. This variation in texture may be correlated with the trend in mechanical proprieties observed in the Cu-MWCNT composites, as (011) orientation is a weak orientation compared to other orientations in Cu [33]. Compressive residual stress is known to enhance the mechanical performance as well as wear resistance by retarding microcrack growth from the surface into the interior [34]. The addition of upto 2 wt. % MWCNTs resulted in the increase of compressive residual stress in the composites as shown in Fig.13 (e). The MWCNTs present at the grain boundaries inhibit grain growth through grain boundary pinning and, therefore, leads to a finer grain structure. However, the compressive residual stress in Cu-3 wt. % MWCNT composite was lower than that achieved in the case of pure Cu due to the agglomeration of MWCNTs at the grain boundaries of the Cu matrix which leads to the formation of pores.

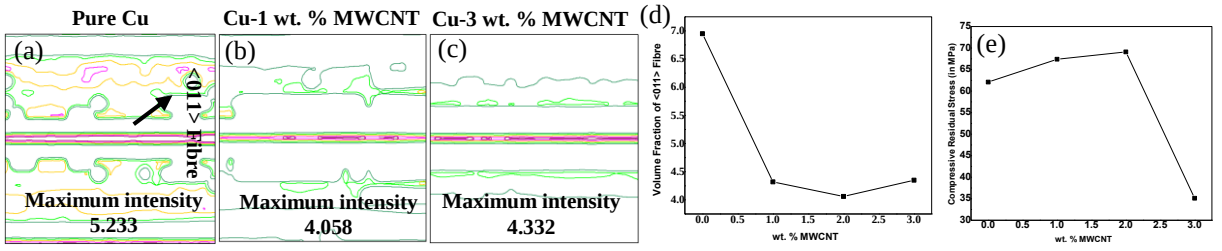

Fig. 13 ODF map (ϕ_2 =0°) of (a) pure Cu (b) Cu-1 wt. % MWCNT (c) Cu-3 wt. % MWCNT composites. The contour levels are at 2.0, 2.4, 2.8, 3.2 and 3.6 times random. (d) Variation of the volume fraction of <011> fibre in Cu in the various Cu-MWCNT composites. (e) Variation of compressive residual stress in sintered pure Cu and in various Cu-MWCNT composites

Conclusions

1. The MWCNTs were found to be homogeneously dispersed in the Cu matrix when the MWCNT content is upto 2 wt. % in the composites. The increase in the loading level of the MWCNTs leads to the agglomeration of the MWCNTs in the Cu matrix.
2. The relative density of the Cu-MWCNT composites shows an increase with the addition of upto 2 wt. % MWCNTs in the Cu matrix. MWCNTs very effectively fill the microvoids in the composite resulting in better densification of the composite. However, the addition of MWCNT beyond 2 wt. % results in a reduction in relative density of the composite due to the agglomeration of the MWCNTs.
3. Cu-MWCNT composites show significant improvement in hardness and wear resistance up to the addition of 2 wt. % of MWCNT. Beyond the addition of 2 wt. % of MWCNT there is a decrease in the both these properties. The enhancement of these properties is achieved due to the homogeneous distribution of the MWCNTs in the Cu matrix when upto 2 wt. % of MWCNT is added and the high interfacial strength at the Cu-MWCNT interface which is achieved by the functionalization of the MWCNTs. The hardness of the Cu-2 wt. % MWCNT composite was found to be 775 MPa and is about 2.15 times that of the sintered pure Cu sample.
4. The addition of MWCNTs to the Cu matrix adversely affects the tensile strength of the Cu-MWCNT composites. The decrease in tensile strength can be attributed to the formation of an interconnected network of MWCNTs which promoted easy fracture of the composites.
5. A dominant <011> fibre was observed in the samples with/without the addition of MWCNTs in the ODF map. However, the intensity of such fibre decreased with the addition of MWCNTs. The volume fraction of <011> fibre was found to decrease with the addition of MWCNTs up to 2 wt. % and shows a rise on further addition of MWCNTs upto 3 wt. %. The residual stresses in the composites are compressive in nature and shows an increase upto the addition of 2 wt. % of the nanofiller.
6. The nature of fracture was found to be ductile for the various Cu-MWCNT composites. MWCNTs are found to be firmly embedded in the Cu matrix in the case of the Cu-MWCNT composites having a lower loading level of MWCNTs, which is also responsible for the improvement of hardness and wear resistance of the composites.

Acknowledgements

We would like to acknowledge the support provided by the various analytical laboratories of Metallurgical and Materials Engineering, Ceramic Engineering Department and Mining Engineering Department, NIT Rourkela. We also thank the support provided by the Central Research Facility, IIT Kharagpur and the Material Science Laboratory, Physics Department, Jamia Millia Islamia.

References

[1] R. Everett, Metal Matrix Composites: Processing and Interfaces, Academic Press, USA, 2012.
[2] K. Prakasan, S. Seshan, J. Mater. Sci. 34 (1999) 5045-5049.
[3] T. Schubert, B. Trindade, T. Weibgarber, B. Kieback, Mater. Sci. Eng. A 475 (2008) 39-44.
[4] T. Laha Y. Chen, D. Lahiri, A. Agarwal, Composites Part A: Appl. Sci. and Manufacturing 40(5) (2009) 589-594.
[5] C. S. Goh, J. Wei, L. C. Lee, M. Gupta, Nanotechnology 17(1) (2005)
[6] A. Agarwal, S. R. Bakshi, D. Lahiri, Carbon Nanotubes: Reinforced Metal Matrix Composites, CRC Press, USA, 2010.
[7] H. Li, A. Misra, Z. Horita, C. C. Koch, N. A. Mara, P. O. Dickerson, Y. Zhu, Appl. Phys. Lett. 95 (2009) 071907.
[8] S. Iijima, Phys. B: Condens. Matter 323(2002) 1-5.
[9] S. Iijima, C. Brabec, A. Maiti, J. Bernholc, J. Chem. Phys. 104(1993) 2089-2092.
[10] S. Iijima, P. M. Ajayan, T. Ichihashi, Phys. Rev. Lett. 69 (1992) 3100-3103.
[11] H. Li, A. Misra, Y. Zhu, Z. Horita, C. C. Koch, T. G. Holesinger, Mater. Sci. Eng. A 523(2009) 60-64.
[12] K.T. Kim, J. Eckert, S. B. Menzel, T. Gemming, S. H. Hong, Appl. Phys. Lett. 92(2008) 121901.
[13] S. J. Yoo, S. H. Han, W. J. Kim, Carbon 61(2013) 487-500.

[14] G. A. Lopez, E. J. Mittemeijer, Scripta Materialia 51(2004) 1-5.
[15] M. E. Mendoza, I. G. Solorzano, T. Aoki, D. J. Smith, Microsc. Microanal. 21(2015) 489.
[16] R. N. Lumley, T. B. Sercombe, G. M. Schaffer, Met. and mat. transactions A 30(2)(1999) 457-463.
[17] B.Lim, C.Kim, B.Kim, U. Sim, S. Oh, B. Suung, J. Choi and S. Baik Nanotechnology 17 (2006)5759-5764.
[18] G. V. Tendeloo, S. Bals, C. Bittencourt, X. Ke, J. Nanotechnol. 4(2013) 77-86.
[19] N. Shpaisman, J. Grinblat, S. Margel, On Mero. Scientific Research 3(2013) 217-223.
[20] K. T. Kim, S. I. Cha, S. H. Hong, Mater. Sci. Eng. A 449-451(2007) 46-50.
[21] D. H. Nam, J. H. Kim, S. I. Cha, S. I. Jung, J. K. Lee, H. M. Park, H. D. Park, S. H. Hong, J. Nanosci. Nanotechnol.14 (2014) 9134-9138.
[22] Y. Kim, J. Lee, M. S. Yeom, J. W. Shin, H. Kim, Y. Cui, J. W. Kysar, J. Hone, Y. Jung, S. Jeon, Nature Communications 4(2013) 1-7.
[23] Y. S. Zhang, Z. Han, K. Wang, K. Lu, Wear 260 (2006) 942-948.
[24] S. R. Dong, J. P. Tu, X. B. Zhang, Mater. Sci. Eng. A 313(2001) 83-87.
[25] M. John, Corrosion and Oxidation. Halsted Press, New York, 1980, pp. 161-194.
[26] C. R. Carpenter, P. H. Shipway, Y. Zhu, Wear 271(2011) 2100-2105.
[27] T. Suzuki, M. Kato, H. Saito, H. Iizuka, J. Solid Mech. Mater. Eng. 5(2011) 348-359.
[28] R. Patil, V. Chatpalli, C. S. Ramesh, Wear Properties of Cu-CNT Nanocomposites, in: S. Bianco (Ed.), Carbon-Nanotubes-From Research to Applications, InTech, United Kingdom, 2011.
[29] J. A. King, M. D. Via, O. P. Mills, D. S. Alpers, J. W. Sutherland, G. R. Bogucki, J. of Composite Materials 46(2011)331-350.
[30] U. F. Kocks, C. N. Tome, H. R. Wenk, H. Mecking, Texture and Anisotropy: Preferred Orientations in Polycrystals and their effects on Materials Properties, Cambridge University Press, UK, 2000.
[31] E. Maawad, H. G. Brokmeier, L. Wagner, Solid State Phenomena 160(2010) 141-146.
[32] M. R. James, J. B. Cohen, The Measurement of Residual Stresses by X-Ray Diffraction Techniques, in: H. Herman (Ed.), Treatise in Material Science and Technology, Academic Press, New York, 1980, pp. 1-62.